

Study of Nonlinear Effects in Electrokinetics

Gaurav Soni[†], Todd M. Squires, Carl D. Meinhart
University of California Santa Barbara, CA 93117, USA

[†]Corresponding author: gsoni@engr.ucsb.edu

Abstract: We present an experimental and numerical investigation of induced charge electroosmosis (ICEO) on a planar electrode surface directly in contact with a high conductivity electrolytic solution. Symmetric rolls of ICEO flow were produced on the electrode by placing it in an AC electric field. The slip velocity was measured for a range of AC voltages and frequencies using micro particle image velocimetry (μ PIV). The slip velocity was also calculated by finite element simulations based on a linear and a nonlinear model of electrical double layer, respectively. The μ PIV measurements were found to be much lower (two and half orders of magnitude) than the velocities predicted by the linear model. The linear model is valid only under Debye Huckel approximation ($\phi \ll k_b T / e = 25$ mVolt at room temperature) which does not hold true for practical situations. The nonlinear model, on the other hand, predicts velocities which are lower than the linear model and closer to the experimental values. The nonlinearity reduces discrepancy between experimental and numerical results by approximately an order of magnitude. The nonlinear model accounts for nonlinear capacitance of the double layer and lateral conduction of charge in the double layer.

Keywords: Electroosmosis, nonlinear capacitance, surface conduction

1. Introduction

Recent applications of microfluidic devices in biology and biochemistry have revived the interest in the study of electrokinetic transport of ionic fluids, charged species and polarizable particles. DC electroosmotic micropumps [1, 2] have been employed in applications such as chromatography [3] and cooling systems for VLSI chips [4]. DC electric field based applications, however, require very high voltages and lead to undesirable effects such as faradaic reactions and joule heating. High frequency AC fields reduce Faradaic reactions significantly. This enables one to design interesting AC electrokinetic applications. For example, dielectrophoresis has been employed for sorting

cells [5-7]; the AC electrothermal effect has been used for speeding heterogeneous bio assays by producing micro stirring [8]; AC electroosmosis [9] has been used as a method of concentrating DNA in a micro-concentrator [10, 11]. AC electroosmosis has also been shown as a mechanism for micro pumping by introducing asymmetry in the electrode design [12-15].

The linear theory of electrokinetics is valid only for very low driving voltages ($\phi \ll k_b T / e = 25$ mVolt) whereas the experiments are generally performed for several volts. As a result, the experiments yield much lower slip velocities than those predicted by the linear theory [16]. Moreover, the experimental velocities do not follow the ϕ_0^2 scaling as predicted by the linear theory [14]. This emphasizes the need for inclusion of nonlinear effects in the existing theory. Olesen et al., 2006 [17] considered presence of nonlinear capacitance of double layer along with faradaic injections in their analysis of ac electroosmotic micropumps.

Induced charge electroosmosis (ICEO) refers to electroosmotic fluid flows that occur on polarizable surfaces as a result of induction of surface charges and subsequent formation of double layer [18, 19]. Existence of ICEO around a cylindrical wire has been experimentally verified [20]. In this paper, we present experimental demonstration of ICEO flow on a planar electrode and a nonlinear numerical analysis of the effect on slip velocity of nonlinear capacitance of the double layer and lateral conduction of charge within the double layer.

1.1 Induced Charge Electroosmosis

ICEO refers to a phenomenon in which a DC or AC electric field induces charge on a polarizable surface (metal or dielectric), and produces an electroosmotic slip by applying a body force on the electrical double layer [18, 19].

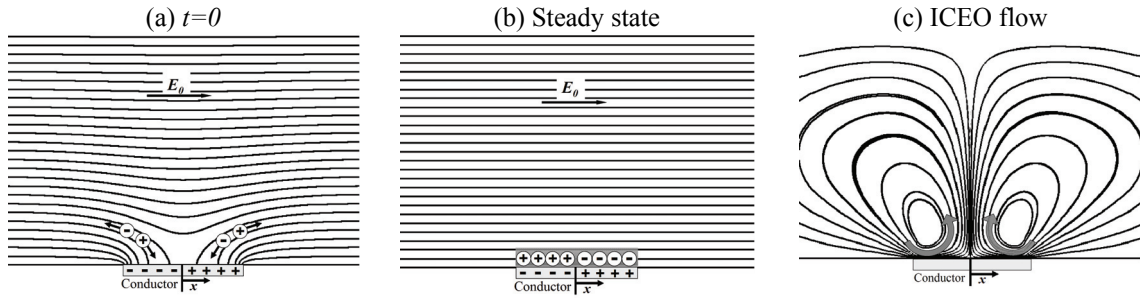


Figure 1: Induced charge electroosmosis on a conducting surface.

Consider a flat conductor surface in contact with an electrolytic solution (figure 1a). When it is subjected to an external DC electric field $E = E_0 \hat{x}$ at $t=0$, the electric field lines intersect the surface at right angles and a charge density is induced on the surface because of charge separation. However, the field lines start changing their configuration as a current, $J = \sigma E$, drives positive ions towards one half of the surface ($x < 0$) and negative ions to the other half ($x > 0$). This process sets up a double layer on the surface which grows as long as a normal electric field exists to drive ions into it. In the steady state, the double layer insulates the surface completely and no electric field lines can penetrate into it. In this state, all the electric field lines become tangential to the surface (figure 1b) and cause an electroosmotic slip directed from the edges toward the center giving rise to two symmetric rolls above the surface (figure 1c). An AC field will drive an identical flow as the change in the direction of the electric field changes the polarity of the induced charge as well.

The slip velocity u_{slip} is given by the Helmholtz Smoluchowski equation,

$$u_{slip} = -\frac{\varepsilon_w}{\eta} \zeta E_{\parallel}, \quad (1)$$

where ε_w and η are respectively the absolute permittivity and viscosity of the ionic solution, ζ is zeta potential of the surface and E_{\parallel} is the electric field component tangential to the surface. ζ is defined as the potential drop from the surface to the bulk right outside the double layer. Assuming that the double layer gets charged completely,

$$E_{\parallel} = E_0, \quad (2)$$

and assuming that the potential on the conductor surface vanishes,

$$\zeta = E_0 x. \quad (3)$$

By substituting these in (1), we get

$$u_{slip} = -\frac{\varepsilon_w E_0^2}{\eta} x, \quad (4)$$

which shows that the velocity is symmetric about the center of the surface, $x=0$, and the maximum slip velocity occurs at the left and right edges of the surface. If the width of the surface is w then the maximum slip velocity is of the order $\varepsilon_w E_0^2 w / 2\eta$. It should be noted that the above analysis is valid only for very low zeta potentials such that the nonlinear effects are absent.

According to (4), u_{slip} depends on the square of the electric field which implies that an AC field also drives a similar flow as long as the frequency, ω , is low enough that the double layer has time to form,

$$\omega < \tau_c^{-1}, \quad (5)$$

where τ_c is the characteristic double layer charging time defined as

$$\tau_c = \frac{\varepsilon_w w}{\sigma \lambda_D} = \frac{\lambda_D w}{D}. \quad (6)$$

Here, λ_D is the double layer thickness, D is the diffusivity of the ions and σ is the electrical conductivity of the solution. Following are the definitions of σ and λ_D ,

$$\sigma = 2n_0 (\hat{z}e)^2 D / k_B T, \quad (7)$$

and

$$\lambda_D = (\epsilon_v k_B T / 2n_0 (\hat{z}e)^2)^{1/2}, \quad (8)$$

where n_0 is the number density of the ions in the bulk, \hat{z} is the valence of the ions, k_B is the Boltzmann constant, T is the temperature and e is the charge of an electron.

2. Experimental Details

ICEO experiments were performed in a microfluidic device which simply consisted of three parallel 200 μm wide planar electrodes laid on a glass substrate. The middle electrode is denoted as the gate electrode whereas the outer two electrodes are denoted as the driving electrodes. The separation between the two driving electrodes, as measured from their respective inner edges, is 0.8 mm (figure 2) and the gate electrode is located symmetrically between them. Experiments were performed in a 125 μm deep closed flow chamber whose sidewalls were made of PDMS. The flow chamber and the electrodes are longer in one direction than the other; therefore, only a two dimensional cross section of the flow chamber (shown in figure 2) was considered in our numerical simulations.

An ionic solution (1 mM KCL, 150 $\mu\text{Siemen/cm}$) was used as the working fluid. The solution was seeded with 700 nm florescent polystyrene particles (Duke Scientific, Fremont, CA) for flow tracing. The flow velocity was measured using micro particle image velocimetry (μPIV) method [21-23].

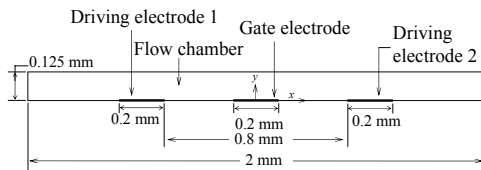


Figure 2: Cross section of the flow chamber.

2.1 Velocity Measurement

Figure 3 shows a μPIV vector field on the gate electrode for a driving-voltage-amplitude of $\phi_0 = 9$ volt and a frequency of $f = 163$ Hz in 1 mM KCl solution. The $x-z$ plane represents the top surface of the electrode. The average velocity variation in the x direction was calculated by averaging the vectors in the z

direction (Figure 4). The fluid flows symmetrically from the two edges ($x = \pm 100 \mu\text{m}$) towards the center of the gate ($x = 0$). The velocity is highest close to the edges and zero at the center, as predicted in the previous section.

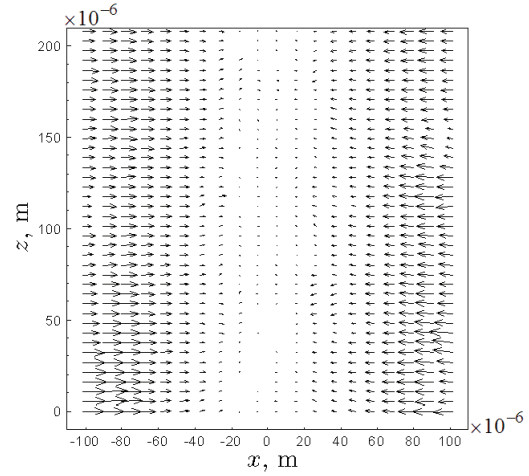


Figure 3: Vector field on the gate electrode for $\phi_0 = 9$ volt and $f = 163$ Hz in 1 mM KCl solution.

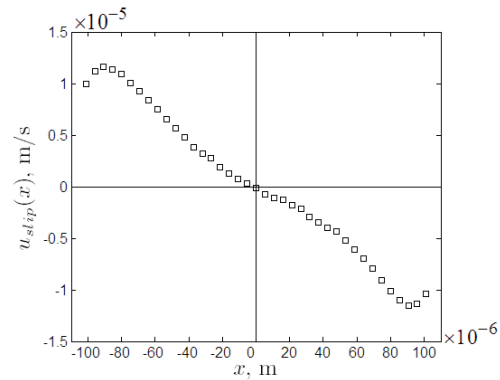


Figure 4: Average slip velocity along the width of the gate electrode $\phi_0 = 9$ volt and $f = 163$ Hz in 1 mM KCl solution.

3. Theory

3.1 Nonlinear Formulation

The nonlinear capacitance establishes a nonlinear relationship between the charge and the zeta potential. The other nonlinear effect, surface conduction redistributes the double layer charge and thus more charge has to be brought into the double layer for replenishment; in other words, more electric field lines have to be normal to the surface. Surface conduction can take place when the zeta potential has a large

lateral gradient along the width of the electrode.

Various field quantities were non-dimensionalized as follows,

$$(\tilde{x}, \tilde{y}) = (x, y) / w, \quad (9)$$

$$(\tilde{u}, \tilde{v}) = \frac{\varepsilon_w \phi_0^2}{\eta w} (u, v), \quad (10)$$

$$\tilde{\phi} = \phi / \phi_0, \quad (11)$$

$$\tilde{\zeta} = \zeta / \phi_0, \quad (12)$$

$$\tilde{t} = t \times f = t \frac{\omega}{2\pi}, \quad (13)$$

$$\tilde{q} = q / q_0, \quad (14)$$

where,

$$q_0 = \frac{\varepsilon_w \phi_0}{\lambda_D}. \quad (15)$$

Here tildes (\sim) represent the nondimensional form of a quantity, x and y are the two spatial coordinates, w is the width of the gate electrode, u and v are the x and y components of the flow velocity respectively, ϕ is the electrostatic potential, ϕ_0 is the amplitude of the driving AC signal, w is the width of the gate electrode, t is the time, f is the driving AC frequency, q is the double layer charge density per unit area and q_0 is the scale chosen for q .

Under the assumption that the bulk is electrically neutral, the bulk electrostatic potential, $\tilde{\phi}$, obeys,

$$\tilde{\nabla}^2 \tilde{\phi} = 0. \quad (16)$$

The insulated walls of the flow chamber are described as

$$\hat{n} \cdot \tilde{\nabla} \tilde{\phi} = 0, \quad (17)$$

where \hat{n} represents the outward surface normal.

While it is desirable to consider the presence of a double layer on all electrode surfaces, we have considered it only on the gate electrode and, for simplicity, ignored it on the driving electrodes. Ignoring the double layer on driving electrodes is a reasonable assumption as the faradaic reactions caused by high driving potentials will disrupt the double layer on the driving electrodes. Thus we can assign known potentials to the driving electrodes with one of them being a sinusoidal function,

$$\tilde{\phi} = \sin(2\pi\tilde{t}), \quad (18)$$

and the other ground

$$\tilde{\phi} = 0. \quad (19)$$

The double layer on the gate electrode can be modeled as a charge conservation equation given by

$$\left(\frac{\omega\tau_c}{2\pi} \right) \frac{\partial \tilde{q}}{\partial \tilde{t}} = \hat{n} \cdot \tilde{\nabla} \tilde{\phi} + \tilde{\nabla}_s \cdot \left(\frac{\sigma_s}{\sigma w} \tilde{\nabla}_s \tilde{\phi} \right), \quad (20)$$

where $\tilde{\nabla}_s$ is the surface gradient operator and σ_s is the surface conductivity with the units of Siemens. The second term on the right hand side represents the surface conduction current. The surface conductivity, σ_s , is more commonly characterized by a non-dimensional number called *Dukhin* number,

$$Du = \frac{\sigma_s}{\sigma w}, \quad (21)$$

which is a strong non-linear function of the zeta potential, $\tilde{\zeta}$, and can be written as follows for a symmetric binary electrolyte [24]

$$Du = \frac{2\lambda_D}{w} \left(1 + \frac{12\pi\varepsilon_w r k_B T}{e^2} \right) \left(\cosh\left(\frac{e\phi_0}{2k_B T} \tilde{\zeta}\right) - 1 \right), \quad (22)$$

where r is the radius of the ions.

For a planar gate electrode in a 2-D system, (20) can be simplified to,

$$\left(\frac{\omega\tau_c}{2\pi} \right) \frac{\partial \tilde{q}}{\partial \tilde{t}} = \frac{\partial \tilde{\phi}}{\partial \tilde{y}} + \frac{\partial}{\partial \tilde{x}} \left(Du \frac{\partial \tilde{\phi}}{\partial \tilde{x}} \right). \quad (23)$$

After \tilde{q} is obtained from (23), one can update the value of $\tilde{\zeta}$ using the following nonlinear capacitance relationship, derived from Gouy Chapman theory for a symmetric binary electrolyte [25],

$$\tilde{\zeta} = -\frac{2k_B T}{e\phi_0} \sinh^{-1} \left(\frac{e\phi_0}{2k_B T} \tilde{q} \right). \quad (24)$$

This value of $\tilde{\zeta}$ can be used to define the bulk potential outside the double layer as shown

below,

$$\tilde{\phi} = \tilde{\phi}_g \sin(2\pi\tilde{t} + \theta) - \tilde{\zeta}, \quad (25)$$

where $\tilde{\phi}_g$ is the amplitude of the potential applied to the gate electrode and θ is the phase gap in the applied gate potential with respect to the driving signal.

3.2 Linear Formulation

If the nonlinear effects are ignored, then the charge conservation equation for the gate electrode does not contain any surface conduction terms and (23) is replaced by

$$\left(\frac{\omega\tau_c}{2\pi} \right) \frac{d\tilde{q}}{d\tilde{t}} = \frac{d\tilde{\phi}}{d\tilde{y}}, \quad (26)$$

and $\tilde{\zeta}$ is related to \tilde{q} through a linear capacitance,

$$\tilde{\zeta} = -\tilde{q}. \quad (27)$$

The rest of the formulation is the same as presented in section 3.1.

3.3 Slip Velocity

The nondimensional slip velocity on the gate electrode is given as

$$\tilde{u}_{slip}(\tilde{x}, \tilde{t}) = -\tilde{\zeta} \tilde{E}_x = \tilde{\zeta} \frac{\partial \tilde{\phi}}{\partial \tilde{x}}, \quad (28)$$

where \tilde{E}_x is the bulk tangential electric field. The time averaged value of the slip velocity is obtained by integrating over one period of oscillation,

$$\langle \tilde{u}_{slip} \rangle = \int_0^1 \tilde{u}_{slip}(\tilde{x}, \tilde{t}) d\tilde{t}. \quad (29)$$

4. COMSOL Implementation

A 2D implementation of the nonlinear model is shown in figure 5. In order to solve for \tilde{q} , a PDE in weak form (representing (23)) was implemented on the gate electrode. $\tilde{\zeta}$ was calculated from \tilde{q} using the nonlinear capacitance (24). This value of $\tilde{\zeta}$ was used for

defining the bulk boundary condition (25) on the gate. $\tilde{\zeta}$ was calculated a second time as $\tilde{\zeta}_i = \tilde{\phi}_g \sin(2\pi\tilde{t} + \theta) - \tilde{\phi}$, in order to be used in the expression for Du (22) (see figure 5). These two separate calculations of $\tilde{\zeta}$ were found necessary to make the cyclic flow of information stable. The time dependent slip velocity, \tilde{u}_{slip} , was calculated from (28), not shown in figure 5.

The problem was solved using a time dependent solver over several periods of oscillations until periodic solutions converged. After the calculations of \tilde{q} , $\tilde{\phi}$ and \tilde{u}_{slip} were complete, the time averaged slip velocity was obtained by integrating a differential form of (29) on the gate electrode, implemented as a weak form PDE,

$$\frac{d}{d\tilde{t}} \langle \tilde{u}_{slip} \rangle = \tilde{u}_{slip}(\tilde{x}, \tilde{t}). \quad (30)$$

Near the end points of the gate electrode, a minimum element size of 1e-2 (nondimensional units) and an element growth rate of 1.1 were used. The problem was solved with a total of 1700 elements. Lagrange quadratic elements were used with non-ideal weak constraints for all the equations.

4.1 Parameters

Following are the constants used in simulations.

w	200 μm
D	$2\text{e-}9 \text{ m}^2/\text{s}$
z	1
e	$1.60\text{e-}19 \text{ Coulomb}$
ϵ_w	$7.08\text{e-}10 \text{ F/m}$
η	$1\text{e-}3 \text{ Pa-s}$
r	1 A°
k_B	$1.38\text{e-}23 \text{ J/K}$

For 1 mM KCl solution, one can obtain $\lambda_D = 9.75 \text{ nm}$ from (8) and $\tau_c = 0.975 \text{ ms}$ from (6). The corresponding frequency is $(2\pi\tau_c)^{-1} \approx 163 \text{ Hz}$. When simulating the symmetric ICEO flow, the gate is assigned a nondimensional potential, $\tilde{\phi}_g$, of 0.5 because it is symmetrically placed between the two driving electrodes. The phase, θ , is taken to be zero. These values of $\tilde{\phi}_g$ and θ represent the floating potential of the gate electrode.

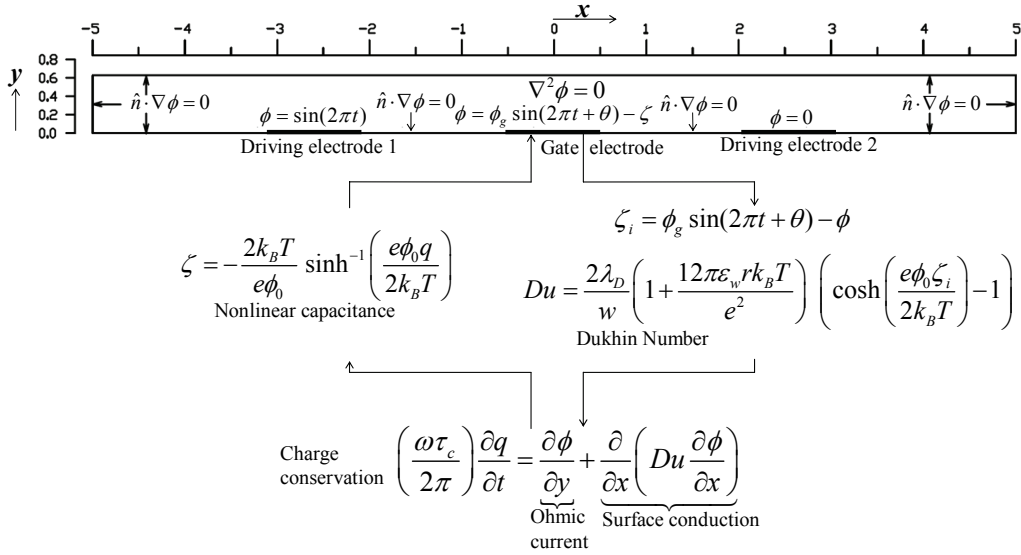


Figure 5: Implementation of the nonlinear double layer model in COMSOL. All geometric dimensions, equations and boundary conditions are nondimensionalized. Tildes (\sim) have been dropped for simplicity.

5. Results

5.1 Variation along the Gate

The numerical simulations in this section were conducted for $\phi_0 = 9$ volt and $f = 163$ Hz in 1 mM KCl solution. These parameters were chosen to match the experimental conditions of Figure 4.

Figure 6 shows variation of $\tilde{\zeta}$ and \tilde{E}_x along the width of the gate electrode. The linear and the nonlinear results correspond to $\tilde{t} = 0.29$ and $\tilde{t} = 0.42$ respectively. These times were chosen as they correspond to the maximum double layer charge for the two models respectively during one full AC cycle ($\tilde{t} = 0$ to 1). a shows that $\tilde{\zeta}$ is zero at the center of the gate ($\tilde{x} = 0$) and has an antisymmetric form about the center. The nonlinear model yields lower values of $\tilde{\zeta}$ and \tilde{E}_x at all points in comparison to the linear results. These lower values of $\tilde{\zeta}$ and \tilde{E}_x cause a significant reduction in the slip velocity, shown in the next section.

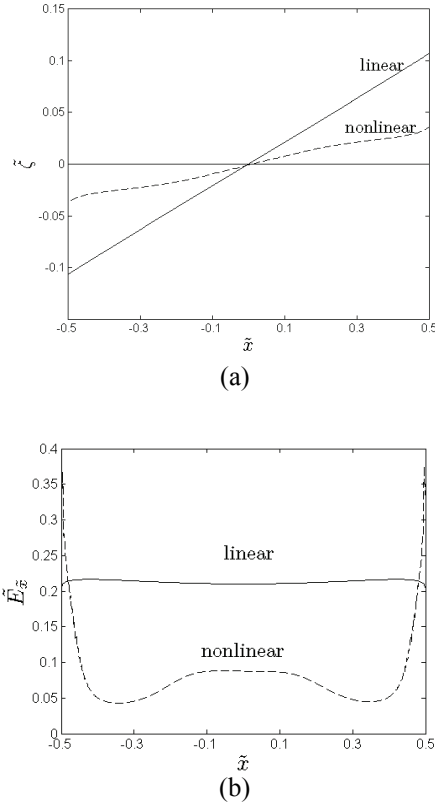


Figure 6: Variations of (a) $\tilde{\zeta}$ and (b) \tilde{E}_x on the gate electrode for $\phi_0 = 9$ volt and $f = 163$ Hz in 1 mM KCl solution for linear and nonlinear formulations at times corresponding to maximum double layer charge.

5.2 Slip Velocity

Figure 7 shows variation of time averaged slip speed $\langle u_{slip} \rangle$ on the gate surface. The linear, the nonlinear and the experimental results have been compared with each other. The linear velocity is approximately two and a half orders of magnitude higher than the experimental measurements. This emphasizes limitation of the linear model in cases where potentials are much above the Debye Huckel limit. The nonlinear model yields an order of magnitude lower velocity in comparison to the linear model. In other words, the nonlinearity reduces the discrepancy between the simulations and the experiments by an order of magnitude.

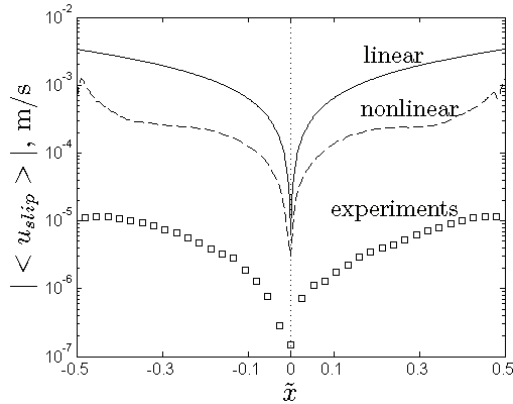


Figure 7: Variation of slip speed $\langle u_{slip} \rangle$ on the gate electrode for $\phi_0 = 9$ volt and $f = 163$ Hz in 1 mM KCl solution.

5.3 Voltage Dependence

Figure 8 shows $\langle u_{slip} \rangle$ at $(\tilde{x} = -0.25, \tilde{y} = 0)$ as a function of the driving voltage amplitude ϕ_0 , for $f = 163$ Hz in 1 mM KCl solution. At low potentials ($\phi_0 \leq 0.5$ volt), the linear and the nonlinear results coincide with each other. As potential grows, the difference between the linear and nonlinear results grows. At high potentials, the nonlinear model reduces the discrepancy between the simulations and the experiments by an order of magnitude. The linear model predicts $\langle u_{slip} \rangle \sim \phi_0^2$ dependence whereas the nonlinear model predicts a relationship with lower slope than $\phi_0 \log \phi_0$. (In figure 8, c is a constant).

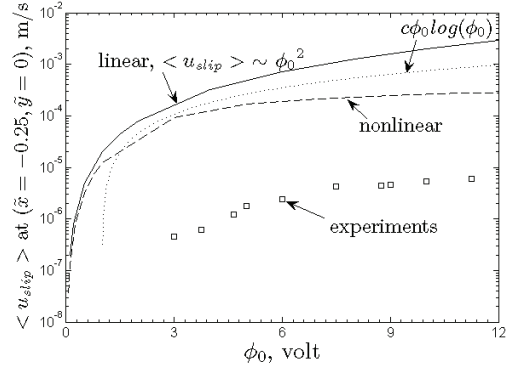


Figure 8: Slip velocity $\langle u_{slip} \rangle$ at $(\tilde{x} = -0.25, \tilde{y} = 0)$ as a function ϕ_0 for $f = 163$ Hz in 1 mM KCl solution.

6. Conclusions

The ICEO slip velocity on a planar surface was measured experimentally and compared to those computed numerically. Slip velocities of $10 \mu\text{m/s}$ were achieved experimentally for an AC signal of 9 volts and 163 Hz (figure 4). No significant flow was observed below 3 volts (figure 8) and thus the experimental potentials fall in a voltage regime much above the Debye Huckel limit. In this regime, the linear theory is certainly not valid and yielded velocities that are two and a half orders of magnitude higher than the experiments (figure 7 and 8). Inclusion of nonlinear capacitance and surface conduction in the theoretical model yielded a reduction of approximately one order of magnitude in the slip velocity as compared to the linear model.

The linear results do not match even qualitatively with the experiments. The linear results show a $\langle u_{slip} \rangle \sim \phi_0^2$ scaling whereas the experimental velocity saturates at higher potentials, showing a scaling inferior to $\phi_0 \log \phi_0$. This behavior is captured qualitatively by the nonlinear results.

The above mentioned nonlinear effects do help in reducing the quantitative and qualitative discrepancy between the numerical and the experimental results but a large difference (one and a half orders) in the slip velocity magnitudes still exists. The reasons behind this large difference remain unclear and open up scope for further modification of the presented theory.

Acknowledgement

This work was supported by the US army research office.

References

1. McKnight, T.E., et al., *Electroosmotically induced hydraulic pumping with integrated electrodes on microfluidic devices*. Analytical Chemistry, 2001. **73**(16): p. 4045-4049.
2. Zeng, S.L., et al., *Fabrication and characterization of electroosmotic micropumps*. Sensors and Actuators B-Chemical, 2001. **79**(2-3): p. 107-114.
3. Jacobson, S.C., et al., *Open-Channel Electrochromatography on a Microchip*. Analytical Chemistry, 1994. **66**(14): p. 2369-2373.
4. Jiang, L.N., et al., *Closed-loop electroosmotic microchannel cooling system for VLSI circuits*. Ieee Transactions on Components and Packaging Technologies, 2002. **25**(3): p. 347-355.
5. Toner, M. and D. Irimia, *BLOOD-ON-A-CHIP*. Annual Review of Biomedical Engineering, 2005. **7**(1): p. 77-103.
6. Hu, X.Y., et al., *Marker-specific sorting of rare cells using dielectrophoresis*. Proceedings of the National Academy of Sciences of the United States of America, 2005. **102**(44): p. 15757-15761.
7. Gascoyne, P.R.C. and J. Vykoukal, *Particle separation by dielectrophoresis*. ELECTROPHORESIS, 2002. **23**(13): p. 1973-1983.
8. Sigurdson, M., D.Z. Wang, and C.D. Meinhart, *Electrothermal stirring for heterogeneous immunoassays*. Lab on a Chip, 2005. **5**(12): p. 1366-1373.
9. Ramos, A., et al., *Ac electrokinetics: a review of forces in microelectrode structures*. Journal of Physics D-Applied Physics, 1998. **31**(18): p. 2338-2353.
10. Wong, P.K., et al., *Electrokinetic bioprocessor for concentrating cells and molecules*. Analytical Chemistry, 2004. **76**(23): p. 6908-6914.
11. Bown, M.R. and C.D. Meinhart, *AC electroosmotic flow in a DNA concentrator*. Microfluidics and Nanofluidics, 2006. **2**(6): p. 513-523.
12. Ramos, A., et al., *Pumping of liquids with ac voltages applied to asymmetric pairs of microelectrodes*. Physical Review E, 2003. **67**(5): p. 11.
13. Seibel, K., et al. *Transport properties of ac electroosmotic micropumps on labchips*. 2003. Cambridge, UK.
14. Studer, V., et al., *An integrated AC electrokinetic pump in a microfluidic loop for fast and tunable flow control*. Analyst, 2004. **129**(10): p. 944-949.
15. Ajdari, A., *Pumping liquids using asymmetric electrode arrays*. Physical Review E, 2000. **61**(1): p. R45-R48.
16. Ramos, A., et al., *Pumping of liquids with traveling-wave electroosmosis*. Journal of Applied Physics, 2005. **97**(8): p. 8.
17. Olesen, L.H., H. Bruus, and A. Ajdari, *ac electrokinetic micropumps: The effect of geometrical confinement, Faradaic current injection, and nonlinear surface capacitance*. Physical Review E, 2006. **73**(5).
18. Squires, T.M. and M.Z. Bazant, *Induced-charge electro-osmosis*. Journal of Fluid Mechanics, 2004. **509**: p. 217-252.
19. Bazant, M.Z. and T.M. Squires, *Induced-charge electrokinetic phenomena: Theory and microfluidic applications*. Physical Review Letters, 2004. **92**(6): p. 4.
20. Levitan, J.A., et al., *Experimental observation of induced-charge electro-osmosis around a metal wire in a microchannel*. Colloids and Surfaces a-Physicochemical and Engineering Aspects, 2005. **267**(1-3): p. 122-132.
21. Meinhart, C.D., S.T. Wereley, and J.G. Santiago, *PIV measurements of a microchannel flow*. Experiments in Fluids, 1999. **27**(5): p. 414-419.
22. Meinhart, C.D., S.T. Wereley, and J.G. Santiago, *A PIV algorithm for estimating time-averaged velocity fields*. Journal of Fluids Engineering-Transactions of the Asme, 2000. **122**(2): p. 285-289.
23. Santiago, J.G., et al., *A particle image velocimetry system for microfluidics*. Experiments in Fluids, 1998. **25**(4): p. 316-319.
24. Lyklema, J., *Fundamentals of interface and colloid science, Volume II: Solid-liquid interfaces*. 2001: Academic press.
25. Bard, A.J. and L.R. Faulkner, *Electrochemical methods, Fundamentals and applications*. second ed. 2001: John Wiley & Sons, Inc.